October 13, 1989

SLAC Proposal E-142

A PROPOSAL TO MEASURE THE NEUTRON SPIN DEPENDENT STRUCTURE FUNCTION

R. Arnold, P. Bosted, S. Rock, Z. Szalata
The American University, Washington, D.C. 20016

T. Chupp
Harvard University, Cambridge, MA 02138

G. Cates, W. Happer, N. Newbury
Princeton University, Princeton, NJ 08544

G . Petratos
University of Rochester, Rochester, NY 14627

R. Gearhart, E. Hughes, R. Pitthan, S. Rokni
Stanford Linear Accelerator Center
Stanford University, Stanford, California 94309

Z. Meziani
Stanford University, Stanford, CA 94305

R. Holmes, D. Kim, K. Kumar, P. Souder
Syracuse University, Syracuse, NY 13210

P. Delheij, O. Hausser, R. Henderson, B. Larson
TRIUMF, Vancouver, B.C. V6T 2A3, Canada

H. Band, J.Johnson, T. Maruyama, R. Prepost
University of Wisconsin, Madison, Wisconsin 53706

Coordinator: Emlyn Hughes (415) 926-4794

Abstract

We propose to measure the the neutron spin dependent structure function in the range $0.04 < x < 0.6$ for $Q^2 > 1$ $(GeV/c)^2$. The experiment requires a 22.66 GeV polarized electron beam scattering off a polarized ^{3}He gas target in End Station A. The scattered electrons will be detected by a two arm fixed spectrometer. We estimate that one month of set-up with beam followed by a month of running at 120 pps will be sufficient to test the Bjorken polarization sum rule to $\pm$ 15 %.

Table of Contents

1. INTRODUCTION

A measurement of the neutron spin dependent structure function is of interest for four reasons. It gives direct information on the contribution of the quark spin content to the nucleon. It tests nucleon models used in supersymmetry and dark matter searches [1]. It serves as a calibration for high energy polarized nucleon scattering such as polarized proton collisions at the SSC. Finally, in conjuction with the measurement of the proton spin dependent structure function, a determination of the neutron spin dependent structure function would test the theoretically well-established Bjorken polarization sum rule [2].

At present, only measurements of the proton spin dependent structure function have been done. Experiments E80 and E130 [3] measured the proton spin dependent structure function in the range from x=.1 to x=.7, and recently the EMC collaboration [4] extended the structure function measurement down to x=.01. The EMC results disagree with the predictions from the Ellis-Jaffe sum rule for the proton [5]. These results indicate that the quarks do not carry the majority of the proton spin content. The number of theoretical papers generated by this result is enormous.

A measurement of the neutron spin dependent structure function would test the Bjorken polarization sum rule for the first time. This sum rule, given below, relates the neutron and proton spin dependent structure functions to the weak coupling constants measured in neutron beta decay.

$$\int_0^1 dx(g^p(x) - g^n(x)) = \frac{1}{6}\frac{g_A}{g_V}(1 - \alpha_s(Q^2)/\pi) = .191 \pm .002$$

The EMC measurement [4] gives

$$\int_0^1 dx g^p(x) = .114 \pm .012(stat.) \pm .026(syst.)$$

With this value, the Bjorken sum rule predicts a large negative contribution to the neutron spin content.

$$\int_0^1 dx g^n(x) = -.077 \pm .029$$

The measurement of the neutron spin dependent structure function also would test independently the Ellis-Jaffe sum rule for the neutron, which predicts that

$$\int_0^1 dx g^n(x) = -.002 \pm .005$$

In short, a measurement of the neutron spin dependent structure function would be a second independent test of the Ellis-Jaffe sum rule and a first test of the Bjorken sum rule in which the neutron results are included.

SLAC has a long history of experience in both the study of deep inelastic e^- scattering and in polarized e^- beams. High current polarized e^- beams are still feasible for a fixed target experiment at the LINAC. Advances in the development of polarized ^{3}He gas targets indicate that these targets would be the most promising for a SLAC measurement of the neutron spin dependent structure function. The theoretical uncertainty in extracting the neutron spin dependent structure function from the ^{3}He spin dependent structure function is expected to be small. The event rate of a e^- ^{3}He scattering experiment are high enough that a precision experiment can be done in a one month run using a large acceptance spectrometer.

2. THE BEAM

We propose to use the polarized GaAs source which is presently being commissioned for the SLC [6]. Table 1 summarizes the parameters of the beam that are needed. A new source laser with a longer pulse length (1.5 μsec) will need to be installed. Otherwise, no change from th SLC polarization set-up should be necessary. Polarization at 42 % is achieved in the laboratory with the cathodes that presently exist.

Helicity reversal of the electrons is achieved by reversing the circular polarization of the pump laser similar to the SLAC parity violating experiment [7]. The reversals can be done on a pulse to pulse basis.

Polarization of the e^- beam will be measured with a Moller polarimeter to an

Table 1. Beam parameters

Energy	22.66 GeV
Polarization	40 %
Intensity	5 x 10^{11} e^- / pulse
Pulse rate	120 Hz
Pulse length	1.5 μsec

accuracy of $\pm$ 5 %. The polarimeter will be constructed for End Station A using the existing designs developed for the SLC.

3. THE TARGET

The recent development of high density polarized ^{3}He gas targets have made ^{3}He the preferred target for a SLAC measurement of the spin dependent structure function of the neutron. The dilution factor, the ratio of the number of polarized nucleons to the total number of nucleons is 1/3 for ^{3}He, ignoring background corrections from extraneous material. This is about three times higher than for solid state targets.

The SLAC target will be based on the technique of ^{3}He polarization by spin exchange with a high density laser optically pumped Rb vapor [8]. The physics of spin exchange in the ^{3}He-Rb system, and other closely related alkali-metal noble-gas systems, has been extensively studied, [9-14] making it possible to project the achievable target parameters which are summarized in Table 2. This technology has been successfully applied in recent experiments at Los Alamos and TRIUMF. Also, extensive tests at the Princeton cyclotron and the Bates Linac have provided detailed quantitative understanding of a variety of effects that will be important to operation in the SLAC beam. In the Los Alamos experiment, [15-17] epithermal neutrons were polarized after passing through longitudinally polarized ^{3}He, and in the Triumf set up [18] a 300 MeV polarized proton beam was used to study the spin-momentum correlations of nucleons in ^{3}He using knockout reactions. The TRIUMF

target had a density of 0.8×10^{20} atoms/cm^3, a volume of 17 cm^3, a length of 8.5 cm, and a ^{3}He polarization of 60%. The SLAC target will be similar in design, but will have twice the target volume and therefore require twice the laser power. The major elements of the SLAC target system are shown in figure 1. The target cell consists of a cylindrical glass cell containing a ^{3}He density of 3×10^{20}cm^{-3} (≈ 10 atmospheres at 300K), a density of N_2 or H_2 of 2 to 4 times 10^{18} cm^{-3} ($\approx 50 - 100$ Torr), and several milligrams of rubidium metal. The N_2 or H_2 is necessary to non-radiatively quench the Rb excited state populated by the absorption of laser light. The cell is heated to $\approx 180°$C to obtain the desired number density of rubidium vapor. The magnetic field of about 30G, produced by Helmholtz coils, establishes an axis of quantization for polarization and dominates the effects of magnetic field gradients [19,20] in the vicinity of the target. The lasers for optical pumping will be two solid state titanium-sapphire lasers, each pumped by an argon-ion laser and producing greater than 8 watts of power.

Table 2. SLAC ^{3}He Target Cell

^{3}He density	3×10^{20} /cc
Polarization	50 %
Polarization direction	longitudinal
cell length	30 cm
cell volume	30 cc
N_2 density	8×10^{18} /cc
Rb density	6×10^{14} /cc
Glass window thickness	2 x 0.10 mm
Glass side walls	0.5 mm
Temperature	180 °C

The ^{3}He nuclear polarization will be measured to an accuracy of 5% by using

either NMR adiabatic fast passage (AFP) [8], or through the observation of the frequency shift that the polarized ^{3}He will cause in the EPR resonance line of the Rb [21]. The polarization of the electron beam will be reversed on a pulse to pulse basis, thereby making occasional flips of the target polarization sufficient for the control of systematic errors. Polarization reversal of the ^{3}He can be accomplished using AFP or through the rotation of the static magnetic field. We note also that when the ^{3}He is initially polarized, the polarization direction can be produced parallel or anti-parallel to the magnetic field.

A simplified expression for the equilibrium polarization of a ^{3}He cell is given by

$$P(\ ^3\mathrm{He}) = P(\mathrm{Rb})\frac{\gamma_{SE}}{\gamma_{SE} + \Gamma_{Beam} + \Gamma_0} \tag{1}$$

where P(Rb) is the average polarization of the Rb vapor, $\gamma_{SE} \approx 1/4$ hr is the spin exchange rate between the ^{3}He and the Rb vapor, $\Gamma_0 < 1/40$ hr, is the ^{3}He spin relaxation rate due to wall collisions and magnetic field gradients, $\Gamma_{Beam} \approx 1/18$ hr is the ^{3}He spin relaxation due to the ionizing effects of the beam. The key to obtaining a high ^{3}He polarization is to arrange for $\gamma_{SE} \gg \Gamma_{Beam} + \Gamma_o$. We note that $\gamma_{SE} = \langle v\sigma_{SE}\rangle$[Rb], where $\langle v\sigma_{SE}\rangle$ is the velocity averaged binary spin exchange cross section. We can obtain any desired value of γ_{SE} by adjusting the Rb number density. [8]To obtain the quoted value of $\gamma_{SE} = 1/4$ hr, we will operate at a Rb number density of about 6×10^{14} cm^{-3}. The equilibrium polarization with the electron beam will be greater than 50%, and it will require about 8 hours of optical pumping prior to bombardment.

The Rb number density dictates the laser power that is necessary for a given target volume. We find that 120 mW/cm^3 of power is needed for the SLAC target. Enough laser power must be available in order to overcome the loss of angular momentum of the photons due to spin destroying Rb-Rb collisions. The required laser power is proportional to the volume and is the only real limit to the size of the target [8]. This has been demonstrated over a range of volumes from 1 to nearly 20 cm^3. For the SLAC target we will need a total of 8 watts at 795 nm. This currently requires two Ti-sapphire lasers each of which is pumped by a 20 Watt argon-ion

laser. However, the demonstrated capabilities of Ti-sapphire lasers are advancing rapidly and it may soon be possible to achieve the required 8 watts with a single laser system.

The depolarizing effects of the electron beam on the ^{3}He are well understood both theoretically [22,23] and experimentally [24,25] and will not pose a problem. The expectation for the SLAC target is a beam induced ^{3}He relaxation time of about 18 hours.

The ionization due to the electron beam affects optical pumping. We are thus planning to separate the region in which the ^{3}He is polarized from the region in which the ^{3}He is bombarded with the electron beam. There are at least two solutions to this problem. For the Bates experiment, a multi-chamber target cell has been developed, [25]as is illustrated in figure 2. The ^{3}He diffuses continuously between the pumping cells and the target cell. The transfer tubes that connect the pumping and target cells allow the ^{3}He atoms to diffuse in a few minutes and maintain a thermal gradient to keep the Rb vapor density negligible outside of the pumping cell. This target design has been tested with low laser power (up to 1 watt), quantitatively demonstrating the validity of the design. By November, 1989, high power testing with a titanium sapphire laser will be underway. Alternatively, two separate cells could be used — one cell would be used as the target while the other cell would be pumped. A sketch illustrating a simple geometry for the use of two cells is given in Fig. 3. In summary, while the issue of the depolarizing effects of the beam on the Rb vapor needs to be addressed, we already have at least one design solution, and other possibilities exist as well.

Sealed ^{3}He cells containing a ^{3}He density of 10^{20}cm^{-3} ($\approx 3\frac{1}{2}$ atms. at 300K) have been extensively studied. These cells are constructed by using liquid nitrogen to increase the density in the cell when the glass seal is made. The primary reason higher pressure cells have not found wider use is the increased complication of the fabrication process—temperatures lower than 77 °K are needed to obtain higher densities in sealed cells. The optical pumping and spin exchange properties of cells containing ^{3}He densities of $3 \times 10^{20}\text{cm}^{-3}$ are expected to be nearly identical to those

of cells with ^{3}He densities of 10^{20}cm^{-3}. Thin glass windows (thickness about 0.15 mm) have been successfully employed at Bates with 40 μA of 250 MeV electrons. [26] For the SLAC target similar windows will be used, although if necessary, metal windows will be employed. In the past, metal windows have not been used because they cause faster spin relaxation than glass windows. The large volume of the SLAC target results in more flexibility, however, because the windows represent a smaller fractional surface area than is the case in smaller cells.

In summary, the SLAC target appears to be a natural and straightforward application of ^{3}He spin-exchange target technology. Test beams will be available at both Princeton and TRIUMF for studying the effects of ionizing radiation, and we anticipate about 1 year of work for target development.

4. THE SPECTROMETER

We propose to use a set of two spectrometers to detect simultaneously electrons scattered at 4.5° and 7°. Figure 4 shows a layout of the apparatus. The 7° spectrometer, made up of existing magnets B201 and B81, provides a high solid angle acceptance of 0.45 msr averaged over the large momentum range $\Delta p/p \approx 50\%$, as illustrated in Figure 5. This large momentum range permits the collection of data over a wide range of x for the same beam and target conditions. The spectrometer will be run at central momentum settings of 10 GeV/c and 15 GeV/c, providing a range in x of 0.1 to 0.6 for $Q^2 > 5\ GeV^2$. The 4.5° spectrometer is made up of existing magnets B204 and B82, and has a solid angle of 0.15 msr averaged over a momentum acceptance of 50%. In this case, the x range will be from 0.04 to 0.20 for $Q^2 > 1\ GeV^2$, providing some overlap with the 7° spectrometer.

The requirements for the detector package in the 7° spectrometer are that it handle rates of 2 electrons per pulse and about 4 pions per pulse (Figure 6) [27]. We plan to use a gas Cerenkov counter and a segmented lead glass array for electron identification, and a set of MWPCs and a hodoscope array for tracking. The Cerenkov counter will be constructed from the existing 4 m long cylinder used in experiment E130. It will be filled with N_2 at a pressure of 0.27 atmospheres, giving

a pion threshold of 11 GeV, and an electron efficiency of about 95% (3.2 photoelectrons expected). Above 11 GeV, the efficiency for pions would rise rapidly, to 50% at 12 GeV and 70% at 14 GeV. Since the π/e ratio drops rapidly with increasing momentum, the expected 50:1 pion rejection power of the lead glass counter will keep the pion contamination small (less than 5% even above pion threshold in the Cerenkov counter). We plan to use the lead glass blocks from the 8 GeV spectrometer, which have an energy resolution of $\sigma(E)/E = 8\%/\sqrt{E}$. We also plan to use the ten planes of wire chambers and the scintillator hodoscope from the 8 GeV/c spectrometer for tracking and fast timing. With the 2 mm horizontal and 4 mm vertical wire spacing of the wire chambers, we expect to obtain a momentum resolution of better than 1%, and a scattering angle resolution of $\pm$ 0.5 mr. These resolutions are more than adequate to correct for the cross section variation within each x bin. The present electronics for the wire chambers will need to be upgraded in order to reduce the dead time and allow several events per spill to be read out. The wire chamber manufacturers have stated that they could provide the desired electronics cards for a cost of about \$20/wire, or a total cost of \$40K. In order to handle a trigger rate of up to 3/pulse, the signals from the shower counter, Cerenkov, and hodoscope would have to be fanned out to three sets of CAMAC ADC's and TDC's. This will require the acquisition of more electronics modules than are presently available in Counting House A.

The detector package for the 4.5° spectrometer is designed to handle electron rates of less than 5/pulse with an average π/e ratio of 2:1. It will consist of a 3.5 m long Cerenkov counter and a lead glass array to identify electrons. We will use the existing 3.5 meter E122 Cerenkov cylinder with mirrors from the 8 GeV Cerenkov counter. As for the 7° spectrometer, it will be filled with N_2 at a pressure of 0.27 atmospheres, providing a pion threshold of 11 GeV/c. The lead glass array will be composed of the forty 10 by 10 by 25 cm blocks used in experiment NE4. The good ($\sigma(E)/E = 7\%/\sqrt{E}$) resolution of these blocks, combined with the pion rejection power of the Cerenkov counter, will keep the pion contamination below 2% for all kinematic settings. The existing phototubes for the lead glass blocks are

slow and would need to be replaced with faster tubes. Because of the high electron and pion rates per pulse, we propose to use a set of two scintillator hodoscopes for tracking and fast timing. In the horizontal direction, position information only is needed to obtain the scattering angle, so that a single plane of 5cm wide units will give a resolution of a few mr. In the vertical direction, measurements of both position and angle are necessary to achieve the desired momentum resolution of better than 5%. This will require two planes of 1.25 cm wide scintillators separated by 2 m. Coincidences between various combinations of scintillators will determine the momentum, which in coincidence with various scattering angle bins will be recorded in hardware scalers. This scheme will require a substantial investment in new electronics, (e.q. several dozen 16-channel ECL discriminator, coincidence, and scaler modules), as well as building the hodoscopes. For monitoring the efficiency, effective dead time, and pion contamination of the system, information from one of the triggers in each beam burst will be read into the computer. We are presently investigating the possibility of using wire chambers for tracking in the 4.5°, at a substantially reduced trigger rate.

Also we note that the contamination from e^+ background is negligible. The threshold for significant e^+ production with a 22.66 GeV beam is W = 5.5 GeV. No bins in x correspond to such a high value of W.

5. EVENT ANALYSIS

With the experimental conditions given in the previous sections, the event rates and statistical errors on the spin-dependent asymmetries are calculated. Table 3 and Table 4 give the kinematic variables and the cross-sections for the 7° and 4° data, respectively. Figure 7 shows the event rates per pulse as a function of x. The differential cross-section, $d^2\sigma^p$, appearing in these tables is in units of 10^{-30} cm^2/sr and corresponds to

$$d^2\sigma^p = \frac{d^2\sigma}{d\Omega dE^{out}} E^{out}$$

$$d^2\sigma^p = E^{out}\frac{d\sigma^{Mott}}{d\Omega}[W_2 + 2W_1 tan^2(\theta/2)]$$

Table 3. Kinematics and cross-sections for E=22.66 GeV and θ=7°

E^{out}	ν	Q^2	W	D	x	F_2^p	$d^2\sigma^p$
7.0	15.66	2.36	5.28	.7251	.0805	.3201	.1686
7.5	15.16	2.53	5.18	.6999	.0891	.3258	.1809
8.0	14.66	2.70	5.07	.6745	.0983	.3319	.1944
8.5	14.16	2.87	4.96	.6488	.1081	.3333	.2064
9.0	13.66	3.04	4.84	.623	.1186	.3337	.2188
9.5	13.16	3.21	4.73	.5971	.13	.3342	.2323
10.0	12.66	3.38	4.61	.5713	.1422	.3347	.2471
10.5	12.16	3.55	4.49	.5454	.1555	.3352	.2633
11.0	11.66	3.72	4.36	.5197	.1699	.3358	.2811
11.5	11.16	3.88	4.23	.4941	.1856	.3364	.3009
12.0	10.66	4.05	4.10	.4687	.2027	.3358	.3214
12.5	10.16	4.22	3.96	.4435	.2215	.3271	.3360
13.0	9.66	4.39	3.82	.4185	.2423	.3175	.3508
13.5	9.16	4.56	3.67	.3938	.2654	.3069	.3658
14.0	8.66	4.73	3.52	.3694	.2911	.2951	.3805
14.5	8.16	4.90	3.36	.3453	.32	.2780	.3892
15.0	7.66	5.07	3.19	.3215	.3526	.2568	.3918
15.5	7.16	5.24	3.01	.2981	.3898	.2326	.3884
16.0	6.66	5.40	2.82	.2751	.4326	.2002	.3677
16.5	6.16	5.57	2.62	.2524	.4823	.1610	.3270
17.0	5.66	5.74	2.40	.2301	.5408	.1221	.2761
17.5	5.16	5.91	2.16	.2083	.6107	.0808	.2050
18.0	4.66	6.08	1.88	.1868	.6955	.0392	.1127

where W_1 and W_2 are the proton structure functions.

Table 4. Kinematics and cross-sections for E=22.66 GeV and θ=4.5°

E^{out}	ν	Q^2	W	D	x	F_2^p	$d^2\sigma^p$
7.0	15.66	.978	5.41	.7243	.0333	.2890	.8893
7.5	15.16	1.05	5.32	.6990	.0368	.2913	.9448
8.0	14.66	1.12	5.22	.6735	.0406	.2938	1.006
8.5	14.16	1.19	5.12	.6477	.0447	.2965	1.073
9.0	13.66	1.26	5.03	.6218	.0491	.2994	1.146
9.5	13.16	1.33	4.92	.5959	.0538	.3025	1.228
10.0	12.66	1.40	4.82	.5699	.0588	.3058	1.319
10.5	12.16	1.47	4.71	.5440	.0643	.3094	1.420
11.0	11.66	1.54	4.61	.5181	.0703	.3134	1.532
11.5	11.16	1.61	4.50	.4924	.0767	.3176	1.659
12.0	10.66	1.68	4.38	.4669	.0838	.3223	1.802
12.5	10.16	1.75	4.27	.4416	.0916	.3275	1.964
13.0	9.66	1.82	4.15	.4165	.1002	.3330	2.149
13.5	9.16	1.89	4.02	.3917	.1098	.3334	2.320
14.0	8.66	1.96	3.89	.3672	.1204	.3338	2.514
14.5	8.16	2.03	3.76	.3430	.1323	.3343	2.733
15.0	7.66	2.10	3.63	.3192	.1458	.3348	2.983
15.5	7.16	2.17	3.49	.2957	.1612	.3354	3.271
16.0	6.66	2.24	3.34	.2726	.1789	.3362	3.605
16.5	6.16	2.31	3.18	.2498	.1995	.3370	3.997
17.0	5.66	2.38	3.02	.2275	.2237	.3261	4.307
17.5	5.16	2.44	2.85	.2055	.2526	.3128	4.636
18.0	4.66	2.51	2.67	.1839	.2877	.2967	4.981

D is a factor which corresponds to the depolarization of the virtual photon and

is given by:

$$D = \frac{E - \frac{E^{out}}{1+2(1+\nu^2/Q^2)tan^2(\theta/2)}}{E[1 + \frac{R}{1+2(1+\nu^2/Q^2)tan^2(\theta/2)}]}$$

where R=σ_L/σ_T [28].

Given the proposed running time (section 7), figure 8 presents the total event rate for the experiment.

Figure 9 shows the statistical uncertainty on the asymmetry measurement, ΔA_1^n, derived from the event rates of figure 8.

$$\Delta A_1^n = \frac{\delta}{P_e P_t f D}$$

$$\delta = 1/\sqrt{Number\ \ of\ \ events}$$

P_e = beam polarization

P_t = target polarization

f = dilution factor

D = virtual photon depolarization factor

The dilution factor used for calculating figure 9 takes into account the difference between the proton and neutron cross-sections [29]:

$$\sigma^n(x) = \sigma^p(x)(.92 - .883x)$$

The small correction on the dilution factor due to the EMC effect [30] is ignored for this calculation. In short,

$$f = \frac{\sigma^n(x)}{3.86\sigma^p(x) + 2.86\sigma^n(x)}$$

where the extra 1.86 corresponds to the non-^{3}He target material.

Finally, the relationship between the asymmetry A_1^n and the spin dependent

structure function in the scaling limit is given below:

$$g^n(x) = \frac{F_2^n(x)}{2x(1+R)} \frac{A_1^n}{D}$$

Figure 10 shows a comparison of the proton spin dependent structure function measurements from the EMC collaboration and the old SLAC experiments, E80 and E130, with the measurement of the neutron spin dependent structure function proposed in this report. The asymmetry for the neutron spin dependent structure function is assumed to be zero, and the error bars for the neutron points are statistical only. The impact of the 4.5° and 7° data are shown separately.

6. SYSTEMATIC UNCERTAINTIES

The experiment should be limited by systematic uncertainties. Table 5 gives breakdown of these uncertainties. The numbers represent the percentage uncertainty on $\int g_1^n(x)dx$ assuming that it has the value -0.08 as predicted by the Bjorken sum rule in combination with the results of the new EMC data [4].

Table 5. Systematic Uncertainties

A_2	9 %
Beam polarization	5 %
Target polarization	5 %
Dilution factor	5 %
F_2	5 %
R	2 %
Radiative corrections	2 %
Total	14 %

The largest uncertainty comes from not knowing the asymmetry A_2. The rela-

tionship between A_2 and $g_1(x)$ is given below:

$$g_1(x) = \frac{F_2(x)}{2x(1+R)}[A/D + (\sqrt{Q^2}/\nu - \eta)A_2]$$

A conservative bound on the value of A_2 is $|A_2| \leq \sqrt{R}$. Therefore, the uncertainty on $\int g_1^n(x)dx$ due to A_2 is calculable. From measurements of R [28]at the Q^2 of this experiment,

$$\int \frac{(\sqrt{Q^2}/\nu - \eta)A_2 F_2^n(x)dx}{(1+R)x} = 0.007$$

For $\int g_1^n(x)dx$ = -.08, this corresponds to a ± 9 % uncertainty.

The Moller polarimeter measures the beam polarization to ± 5 %. The measurement is inherently limited by a background subtraction of the signal and an uncertainty in the amount of electron spin magnetism.

The target polarization measurement is limited by the uncertainty in the density of ^{3}He in the cell and by local fluctuations in the B-field along the electron beam trajectory compared to the entire ^{3}He volume.

The 5 % uncertainty in the dilution factor is dominated by the uncertainty in the thickness of the glass cell walls. We assume that the wall thickness will be known to ± 10 % of its value (i.e. ± 0.01 mm). Software cuts could possibly reduce the background from the walls.

The last large uncertainty comes from the experimental uncertainty in the determination of the ratio of the neutron to proton structure functions [29]. A 5 % uncertainty in $F_2^n(x)$ gives directly a 5 % uncertainty in $g_1^n(x)$.

Radiative corrections to the asymmetry measurements will add an uncertainty in the extraction of A_1^n. For the proton data in electron scattering [31], these corrections changed the absolute value of A_1^p by .01 to .05, depending on the value of x. If these corrections are known to ± 20 %, then the additional uncertainty on A_1^p coming from the radiative corrections would range from negligible to .01.

The radiative corrections to the neutron asymmetries should be similar but do

depend upon the measured results. An estimate of the external corrections due to the present target cell with 0.1 mm windows and 0.5 mm walls indicate that the radiative corrections will be dominated by the internal rather than the external contributions.

7. PROPOSED RUN

This experiment requires a one month running period of the SLAC LINAC with a total of 90 hours of data recorded on tape per spectrometer. Table 6 lists the breakdown of how these hours would be used. Note that the run time for the 7° and 4.5° spectrometers is the same. We estimate that the experiment will run with an average efficiency of 1/4. And that of this efficient run time, 1/2 of the data will be recorded on tape.

Table 6. Proposed running time

Experimental conditions			
Spectrometer angle	Spect mom setting	x range	Hours
4.5 °	15 GeV	.05 to .2	60
7 °	15 GeV	.15 to .6	60
4.5 °	10 GeV	.04 to .16	30
7 °	10 GeV	.09 to .4	30

We also request a two week test beam run for set up and initial tests.

8. FROM ^{3}He TO THE NEUTRON

The nucleon spin structure of a polarized ^{3}He target is the same as a polarized free neutron target to the extent that the ^{3}He nucleus is in a spatially symmetric S state. In an S state, the proton spins remain anti-parallel in order not to violate the Pauli exclusion principle.

An analysis of quasi-elastic data has revealed that to $\sim$ 90 %, the ^{3}He wavefunction is in a spatially symmetric S state [32]. Figure 11 gives the results of the calculations of partial wave channels of the Derrick-Blatt model [33] used in reference 14. A recent comparison [34] of existing models of the ^{3}He wavefunction showed that all models give the same result for the probability that the neutron polarization is aligned along the ^{3}He polarization. The result of this analysis was that the probability of the neutron spin being aligned is 93 % $\pm$ 1 %, and therefore a 100 % polarized ^{3}He target corresponds to a net neutron polarization of 86 %. The excellent agreement between the models does not justify their validity; however, the results do indicate that to a large extent a polarized ^{3}He target does represent a polarized neutron target. Note that the small ($\sim$ few percent) presence of a polarized proton contribution (D-state ^{3}He) is not significant enough to affect the asymmetry measurement.

A recent paper [35] has calculated the asymmetry measurements of a ^{3}He experiment using the Carlitz-Kaur model of the neutron asymmetry [36] and the Afnan-Birrell ^{3}He wavefunction [37]. The similarity between the neutron and ^{3}He predictions is apparent (see figure 12).

A complete theoretical study of the polarized ^{3}He nucleus and its relation to the polarized neutron has only started. We list the main uncertainties that have been identified:

- uncertainties in the ^{3}He wavefunction
- final-state meson exchange currents (i.e. ρ exchange). which directly affect the asymmetry
- final state meson exchange currents (i.e. π exchange). which contribute to the denominator of the asymmetry
- 3 body forces

For the first uncertainty, we crudely assign an error which is equal to the dif-

ference between the simple case of the spatially symmetric S state ^{3}He nucleus and the more detailed predictions of the ^{3}He wavefunctions. With this error, a 100 % polarized ^{3}He corresponds to a 86 % $\pm$ 14 % polarized neutron.

In principle, vector meson exchange is a dangerous background for this experiment, since it can affect directly the numerator of the asymmetry and especially at low x. For $Q^2 < 1\ GeV^2$, the rate of ρ meson production is $\sim$ 10 % of electroproduction [38]. As Q^2 gets larger, this fractional rate decreases. A number of effects must conspire in order to have a significant impact on the overall theoretical uncertainty. First, there must be a significant difference between polarized ρ production in ^{3}He ($e\rho \rightarrow e\rho$) as compared to the free neutron. Second, the asymmetry from polarized electron ρ scattering must be large. Third, the inclusive production of ρ mesons must be large even at $Q^2 > 1\ GeV^2$. Although we do not estimate the size of ρ exchange, it seems likely that the overall impact on the measured asymmetry will be small even at low x.

The third effect, pion exchange, has been related to the non additivity of the structure functions, EMC effect [30]. Measurements of the ^{3}He and deuterium structure functions show that the two are the same to within 5 % from $0.1 < x < 0.6$ [39]. Since this effect only influences the denominator of the asymmetry and since the EMC effect is $\approx$ 10 % for nucleons in very different nuclei, we believe that this uncertainty is small compared to the first.

We do not try to estimate the correction due to three body forces. Their existence is still controversial, but their impact on the three nucleon system is generally not large [40].

Finally, we note that some other effects indicate that the ^{3}He polarized nuclei represents a reasonable model of a polarized free neutron. First, the magnetic moment of ^{3}He (μ^{3He} = -2.13) and the neutron (μ^n = -1.91) only differ by 11 %.

Second, using a simple model of the three body nuclei [41], it has been shown that

$$\left(\frac{g_A}{g_V}\right)^{3H/3He} = \left(\frac{g_A}{g_V}\right)^{n/p}$$

to within a few percent. The relation given above indicates that the ^{3}H - ^{3}He system is similar to the neutron - proton system, and the results depend primarily on the measurements of the ^{3}H and neutron lifetimes.

In summary, we believe that a 1 σ theoretical error of $\pm$ 20 % ($\pm$ .016) on the Bjorken value of $\int g_1^n(x)dx$ (i.e. -0.08) is a reasonable estimate. Future theoretical efforts directed to this problem should be able to bring down the uncertainty.

9. TESTING SUM RULES

The measurement from this experiment will test the Bjorken sum rule to $\pm$ 15%. Table 7 shows the contributions to this error. Note that $\Delta n = \Delta \int g_1^n(x)dx$ and $\Delta p = \Delta \int g_1^p(x)dx$ and that the 15 % error is equivalent to $\int g_1^p(x) - g_1^n(x)dx = .191 \pm .03$.

Table 7. Test of the Bjorken sum rule

Quantity	Type of uncertainty	Value
Δn	statistical	$\pm$ .004
Δn	systematic	$\pm$ .011
Δn	experimental	$\pm$ .012
Δn	theoretical	$\pm$ .016
Δn	total	$\pm$ .020
Δp	experimental	$\pm$ .021
$\Delta p - \Delta n$	total	$\pm$ .03

The measurement will also test the Ellis-Jaffee sum rule for the neutron. If we find, for example, $\int g_1^n(x)dx$ = -.08 $\pm$ .02 as predicted by the Bjorken sum rule, then

this result would imply a 4 σ discrepancy with the predictions of the Ellis-Jaffee sum rule: $\int g_1^n(x)dx$ = -.002.

10. RESOURCES

The following list gives a breakdown of the projects needed for this experiment and an asignment of the manpower.

	RESPONSIBILITY
BEAM	WISCONSIN
Polarized Electron Source	SLAC
Laser gun upgrade	
Position monitors	
Moller polarimeter	
TARGET	HARVARD
^{3}He cell R & D	PRINCETON
	TRIUMF
Laser system	
NMR system	
Test beam for R & D	
SPECTROMETER	AMERICAN
	ROCHESTER
Magnet set up and alignment	STANFORD
Shielding	SYRACUSE
	SLAC
PWC construction	
Pb-glass counters	
N_2 threshold Cerenkov	
Electronics	
On-line / VAX	

Tapes and Off line Software

Appendix A. Additional R & D efforts

We will investigate a few possibilities for improving the experiment, although these are regarded as non-essential features for the experiment.

1. Install a pulsed Ti-Sapphire laser which could run at 790 nm and give 50 % polarization for the beam rather than the present 40 % polarization.

2. Construct a higher density or larger volume target for increased luminosity. This is a natural extension of the ongoing target research.

3. Study with TRANSPORT the possibility of removing from the data sample events originating in the cell walls. If we can reconstruct the vertex of the event, then we could remove the wall events with software cuts. At 7°, this may be possible. At 4.5°, this procedure will be more difficult.

4. For the high rate data at 4.5°, we may use a 3 dipole spectrometer configuration rather than a 2 dipole spectrometer. The advantage of this scheme is that the background due to scraping will be less. There is a sacrifice in acceptance (a loss of about 20 %) using three dipoles. The 3 dipole configuration would consist of 2 dipole magnets from the 20 GeV spectrometer and one dipole from the 8 GeV spectrometer.

REFERENCES

1. J. Ellis, R.A. Flores, S. Ritz, Phys. Lett. 198B (1987) 393.
2. J.D. Bjorken, Phys. Rev. 148 (1966) 1467; Phys. Rev. D1 (1970) 1376.
3. M.J. Alguard et al., Phys. Rev. Lett. 37 (1976) 1258; 37 (1976) 1261.
4. J. Ashman et al., Phys. Lett. B206 (1988) 364.
5. J. Ellis, R. Jaffe, Phys. Rev. D9 (1974) 1444.
6. D. Blockus et al., Proposal for Polarization at the SLC, SLAC proposal 1986.
7. C. Prescott et al. Phys. Lett. 77B (1978) 347 ; 84B (1979) 524.
8. T. E. Chupp, M. E. Wagshul, K. P. Coulter, A. B. McDonald, and W. Happer, Phys. Rev. **36C** (1987) 2244
9. M.A. Bouchiat, T.R. Carver, and C.M. Varnum, Phys. Rev. Lett. **5** (1960) 373.
10. R.L. Gamblin and T.R. Carver, Phys. Rev. **138** (1965) 946.
11. N.D. Bhaskar, W. Happer, and T. McClelland, Phys. Rev. Lett. **49** (1982) 25.
12. W. Happer, E. Miron, S. Schaefer, D. Schreiber, W. A. van Wijngaarden, and X. Zeng, Phys. Rev. A **29** (1984) 3092.
13. T.E. Chupp and K.P. Coulter, Phys. Rev. Lett. **55** (1985) 1074.
14. M. E. Wagshul, T. E. Chupp Phys. Rev. **40A** (1989) 4447
15. K.P. Coulter, T.E. Chupp, A.B. McDonald, C.D. Bowman, J.J. Szymanski, V. Yuan, G.D. Cates, D.R. Benton, and E.D. Earle, *Neutron Polarization with a Polarized ^{3}He Spin Filter*, submitted to Nucl. Instr. and Meth. in Phys. Res.
16. T.E. Chupp, K.P. Coulter, A.B. McDonald, G.D. Cates, W. Happer, D.R. Benton, J.D. Bowman, C.D. Bowman, V Yuan, J.J. Szymanski, E.D. Earle, **BAPS*33*** (1988).
17. K.P. Coulter, A.B. McDonald, G.D. Cates, W. Happer, D.R. Benton, T.E. Chupp, J.D. Bowman, C.D. Bowman, V. Yuan, J.J. Szymanski, E.D. Earle **BAPS *33*** (1988) 905.
18. O. Hausser *et al.*, TRIUMF Prposal "Heliopolis" for experiment E541 (1988).

19. G.D. Cates, S. Schaefer, and W. Happer, Phys. Rev. A **37** (1988) 2877.
20. G.D. Cates, D. J. White, Ting-Ray Chien, S. R. Schaefer, and W. Happer, Phys. Rev. A **38** (1988) 5092.
21. S. R. Schaefer, G.D. Cates, Ting-Ray Chien, D. Gonatas, W. Happer, and T.G. Walker, Phys. Rev. **A39** (1989) 5613.
22. K.D. Bonin, T.G. Walker, and W. Happer, Phys Rev. **A37** (1988) 3270.
23. K.D. Bonin, D.P. Saltzberg, and W. Happer, Phys Rev. **A38** (1988) 4481.
24. K.P. Coulter, A.B. McDonald, G.D. Cates, W. Happer, and T.E. Chupp, Nucl. Instr. and Meth. in Phys. Res. **A276** (1989) 29.
25. T.E. Chupp, M.E. Wagshul, R.A. Loveman, A.M. Bernstein, W. Fong, A.K. Thompson, D. Tieger, K. von Reden, K.P. Coulter, A.B. McDonald, W. Happer, **AIP conference Proceeding #187** (1988) p.1320.
26. D. Beck, *et al.* Bates Proposal 88-25, Bates Linear Accelerator Center, Middleton MA (unpublished, 1988).
27. D.E. Wiser, Ph.D. thesis, University of Wisconsin, 1977, unpublished.
28. S.Dasu et al., Phys. Rev. Lett. 61 (1988) 1061.
29. J.J Aubert et al., Nucl. Phys. B293 (1987) 740.
30. J.J. Aubert et al., Phys. Lett. 123B (1983) 275.
31. G. Baum et al., SLAC PUB 3079 (1983).
32. B. Blankleider & R.M. Woloshyn, Phys. Rev. C 29 (1984) 538.
33. G.Derrick and J.M.Blatt, Nucl. Phys., 8 (1958) 310.
34. J.L. Friar et al., to be published
35. R.M. Woloshyn, Nucl. Phys. 496A (1989) 749.
36. R.Carlitz and J.Kaur, Phys. Rev. Lett. 37 (1976) 673.
37. I.R.Afnan and N.D.Birrell, Phys. Rev. C 16 (1977) 823.
38. E.D. Bloom et al., Phys. Rev. Lett. 28 (1972) 516.
39. R.G. Arnold et al., Phys. Rev. Lett. 52 (1984) 727.
40. J.L. Friar, proceedings of NEW VISTAS IN ELECTRO-NUCLEAR PHYSICS, (1986) p. 213.
41. T.W.Donnelly and J.D. Walecka, Nucl. Phys. 274A (1976) 368.

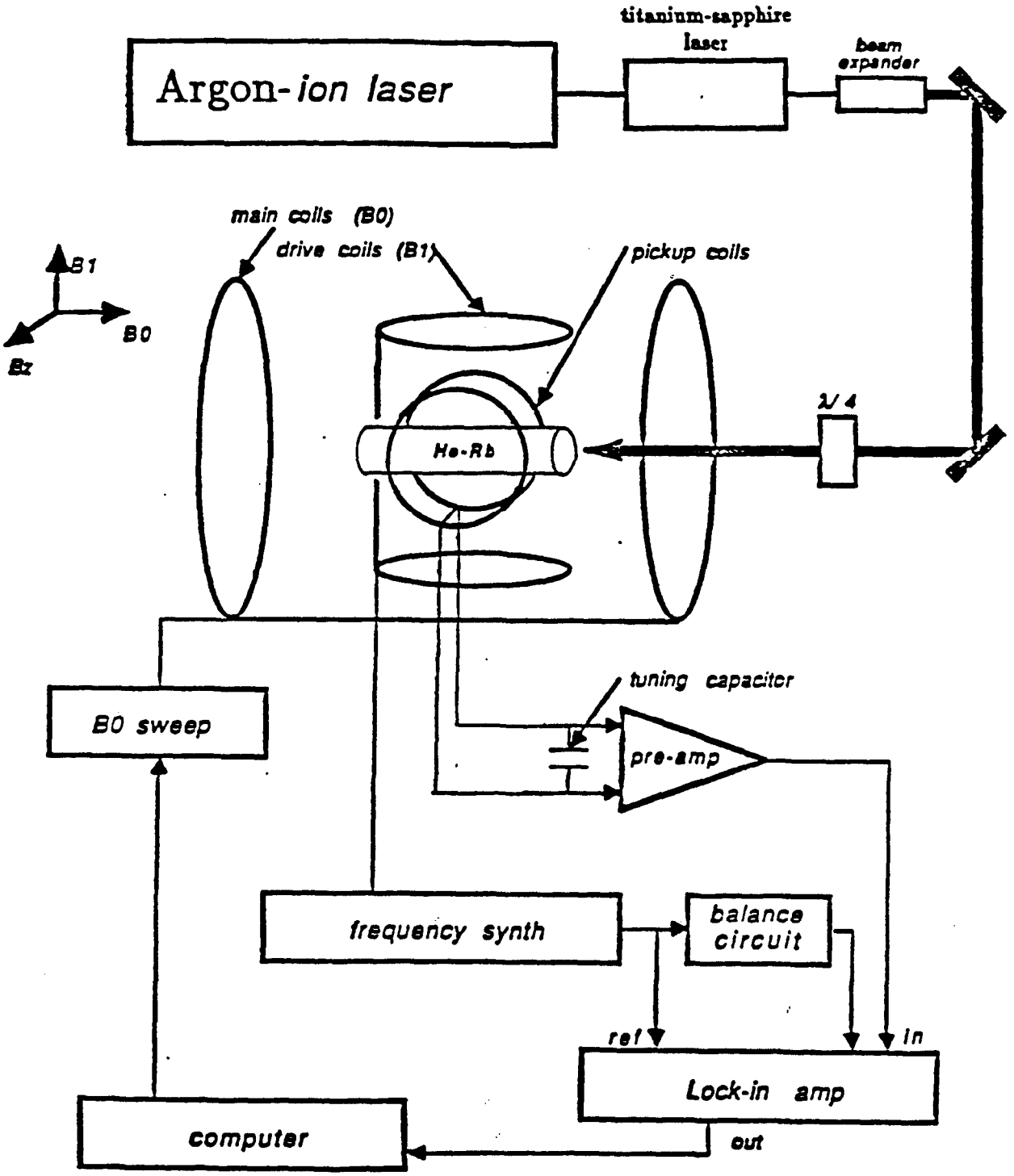
titanium-sapphire laser
Argon-ion laser
beam expander
main coils (B0)
drive coils (B1)
pickup coils
B1
B0
Bz
λ/4
He-Rb
tuning capaciter
B0 sweep
pre-amp
frequency synth
balance circuit
ref
in
Lock-in amp
computer
out

Figure 1

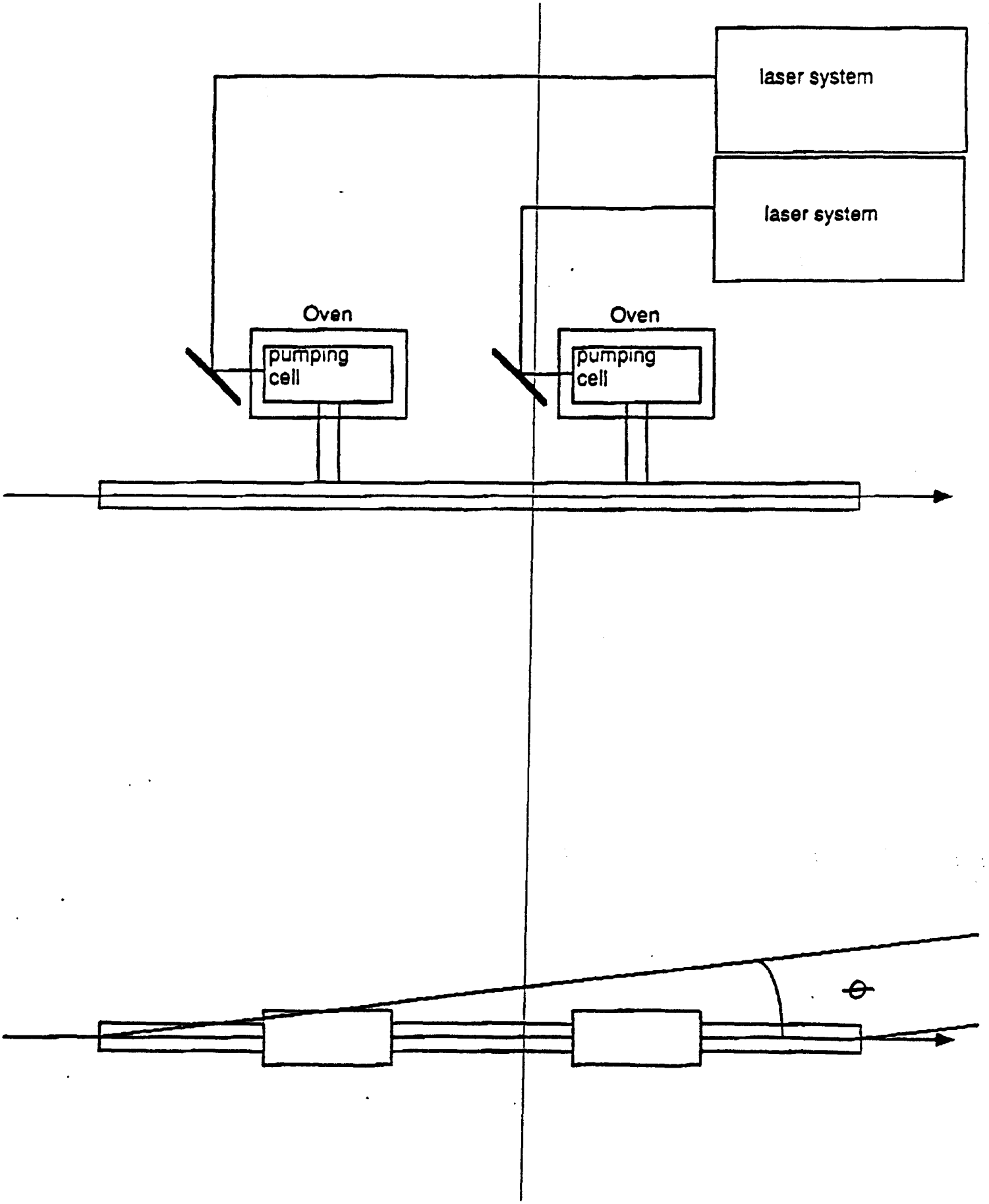
laser system
laser system
Oven
pumping cell
Oven
pumping cell

Figure 2 (a)

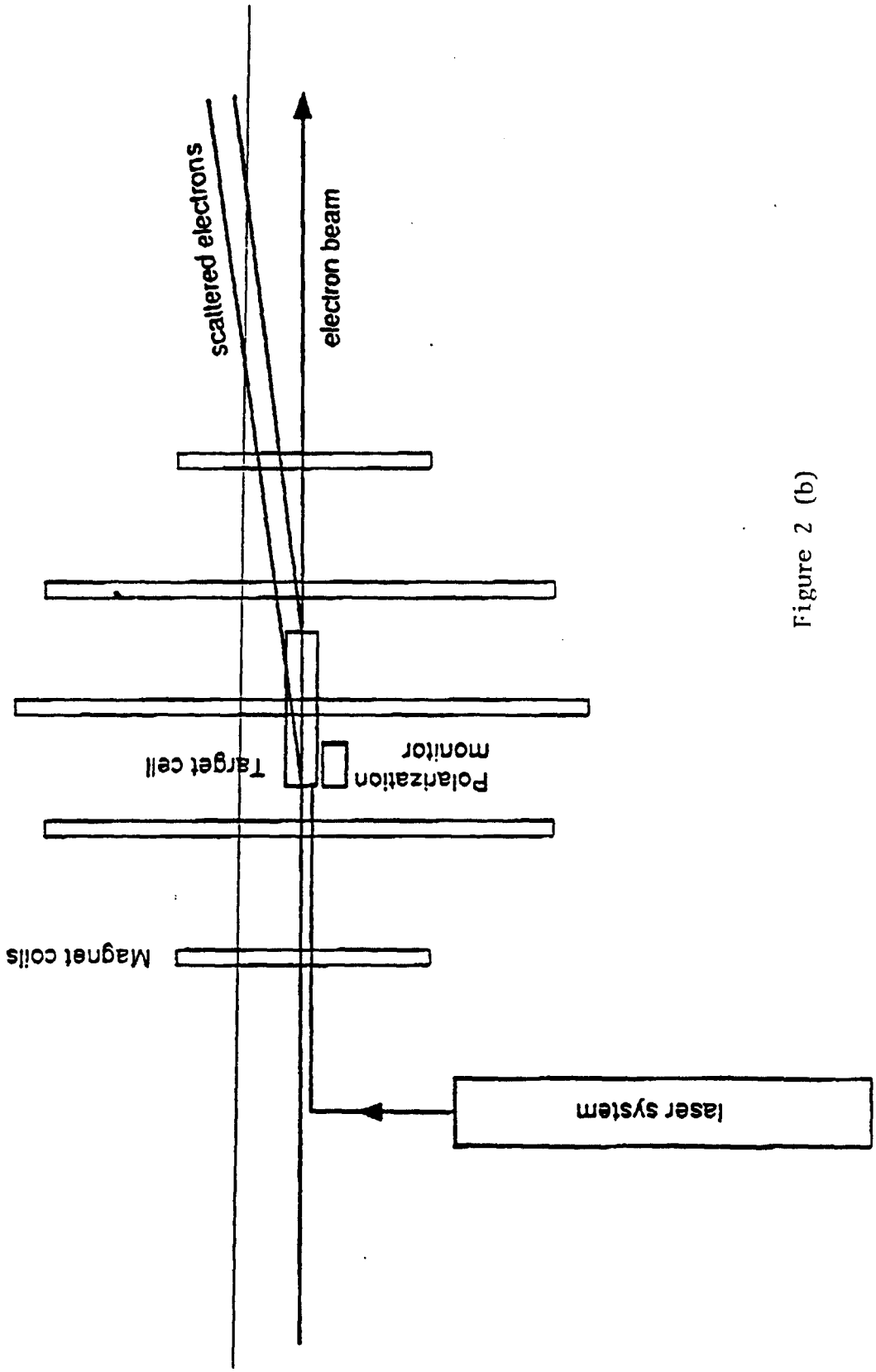
laser system
Magnet coils
Target cell
Polarization
monitor
electron beam
scattered electrons

Figure 2 (b)

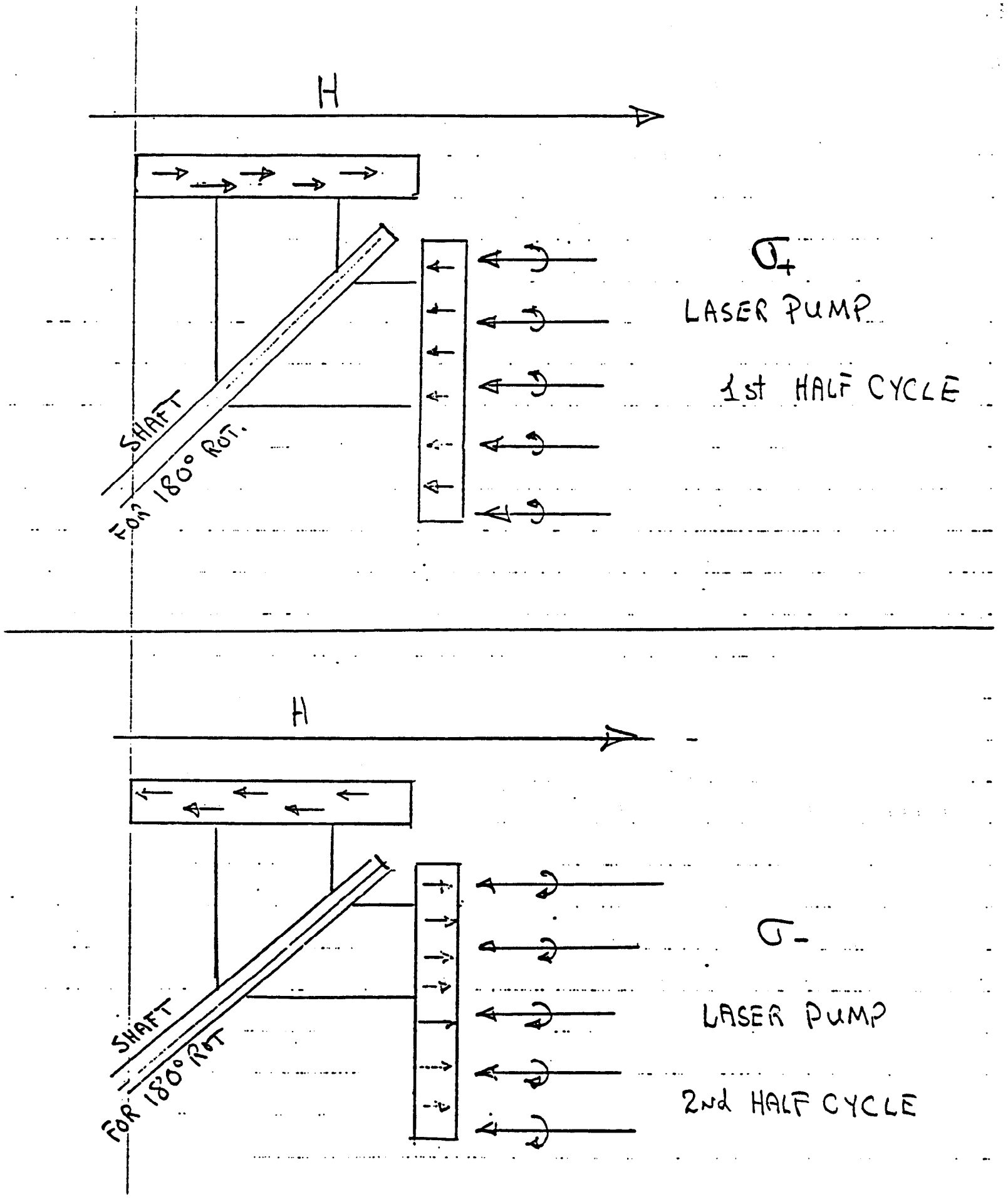
H
SHAFT
FOR 180° ROT.
σ_+
LASER PUMP
1st HALF CYCLE
H
SHAFT
FOR 180° RT
σ_-
LASER PUMP
2nd HALF CYCLE

Figure 3

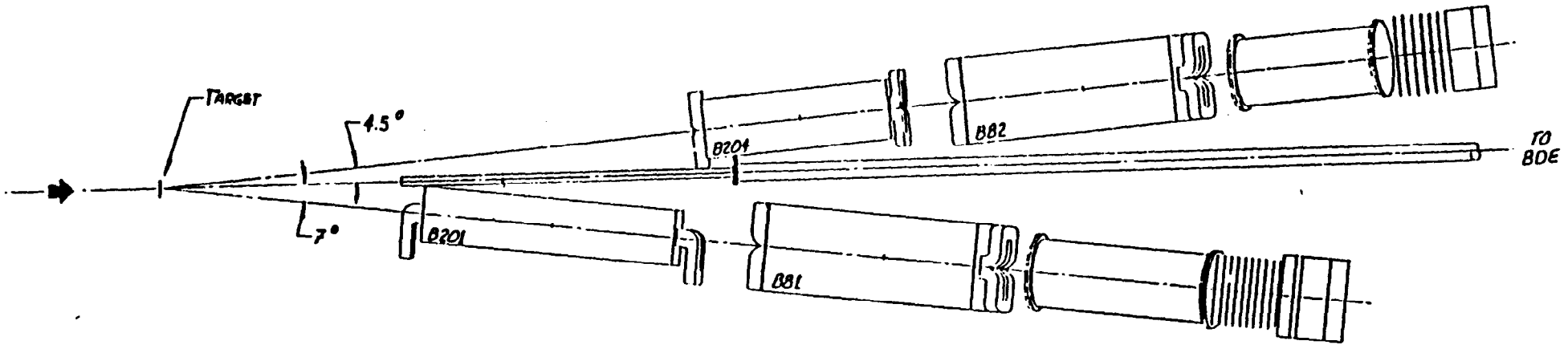

Plan View

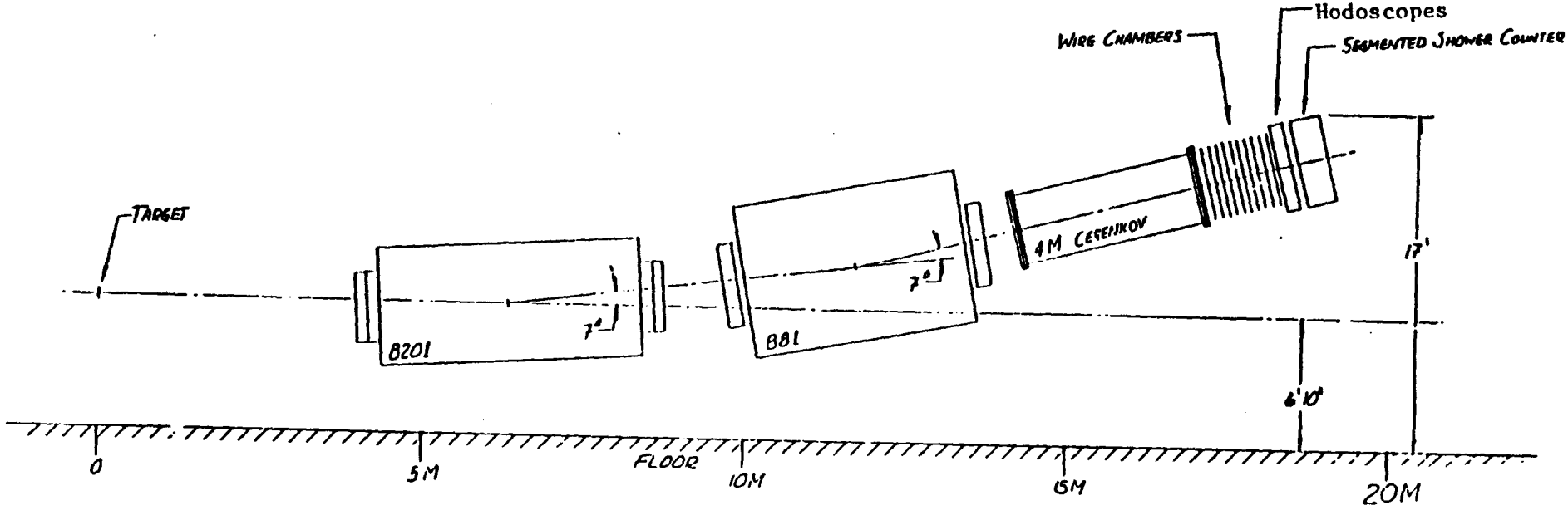

Elevation view (identical for the two arms)

FIGURE 4

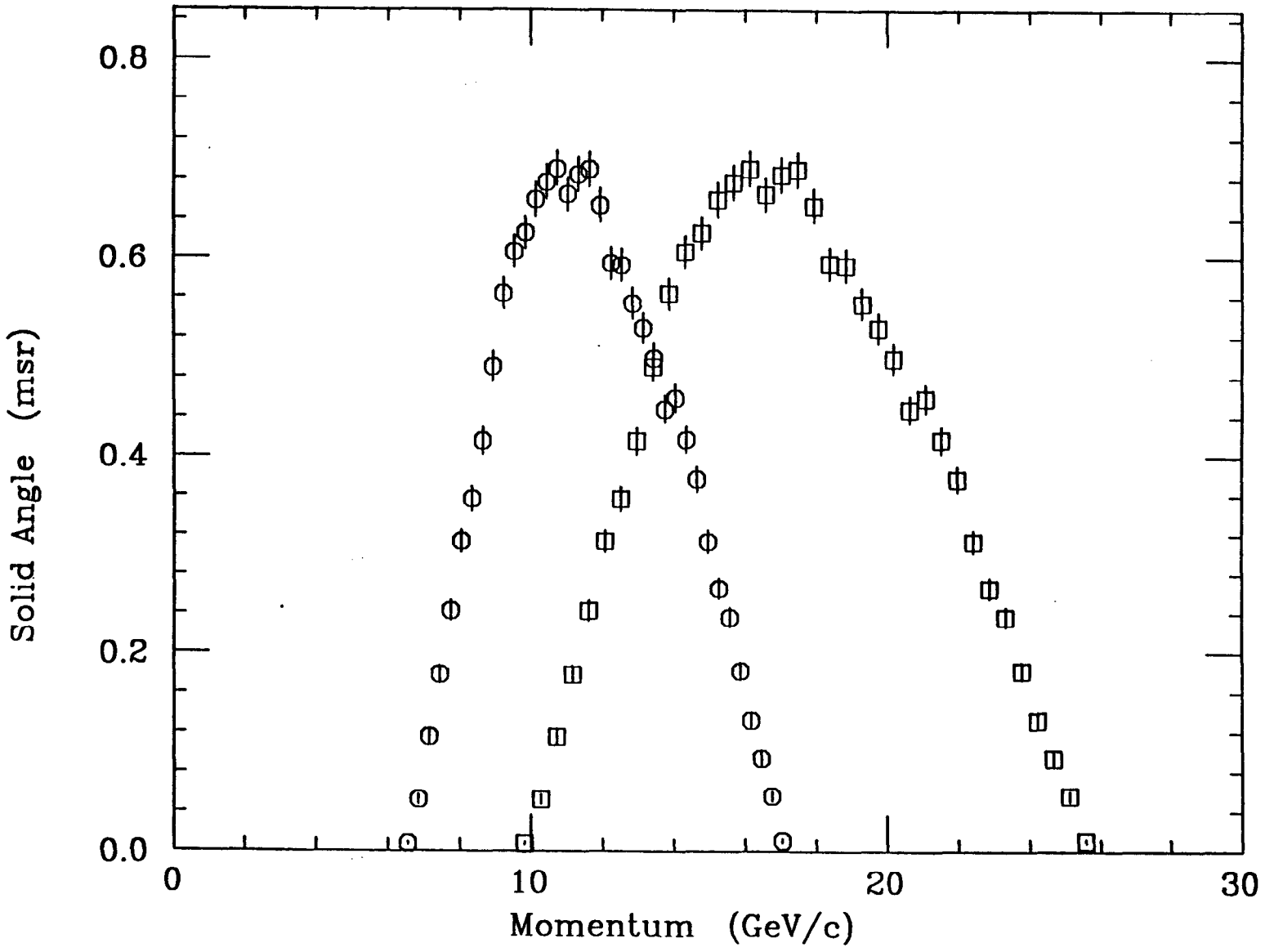

Figure 5

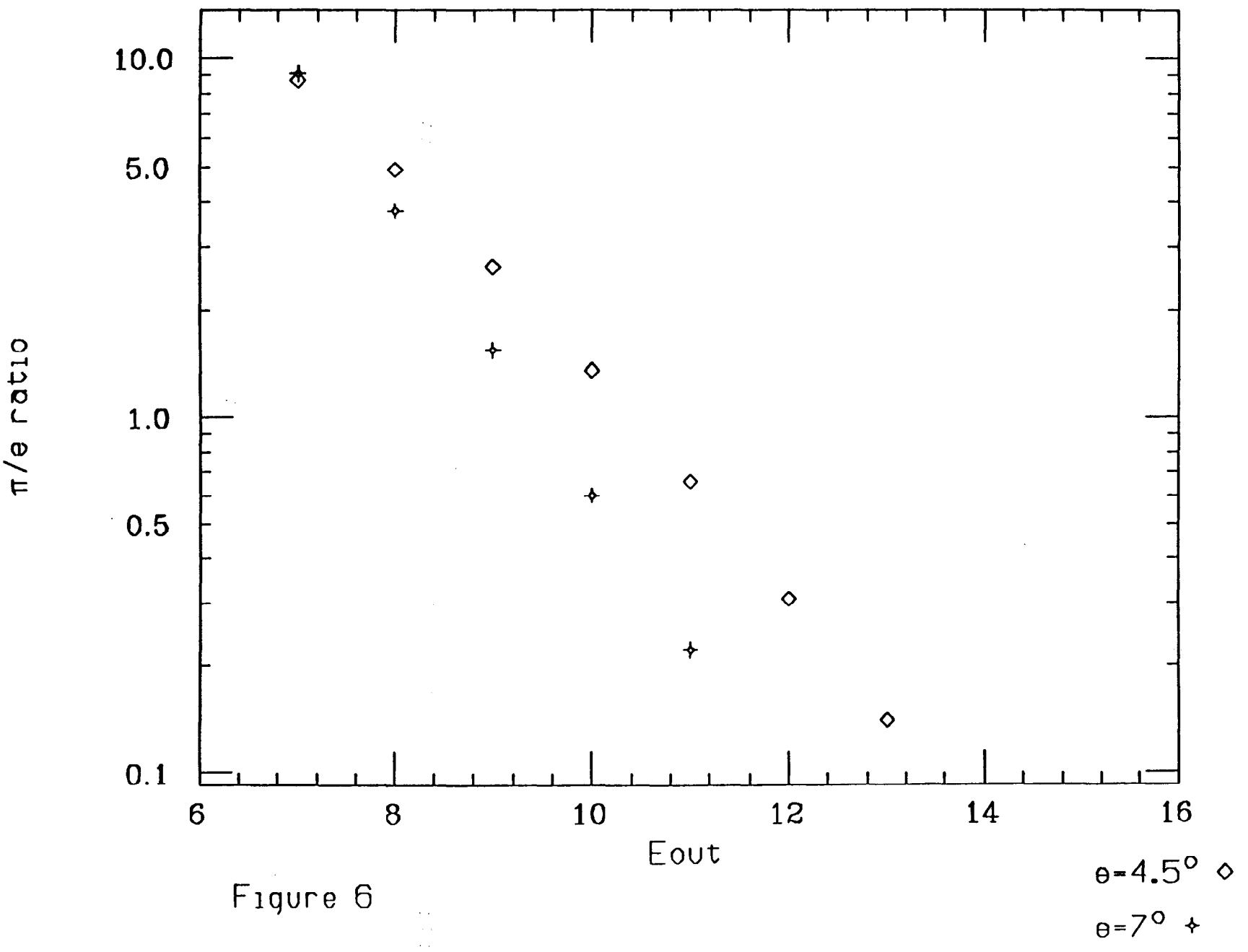
HADRONIC BACKGROUND
10.0
5.0
1.0
0.5
0.1
π/e ratio
6
8
10
12
14
16
Eout
θ=4.5°
θ=7°

Figure 6

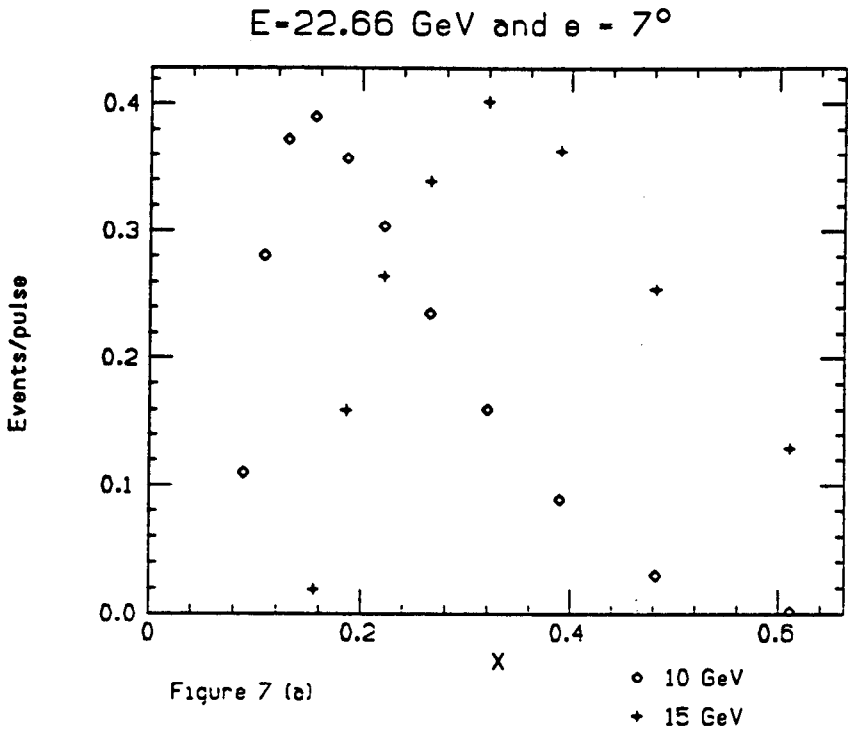

Figure 7 (a)

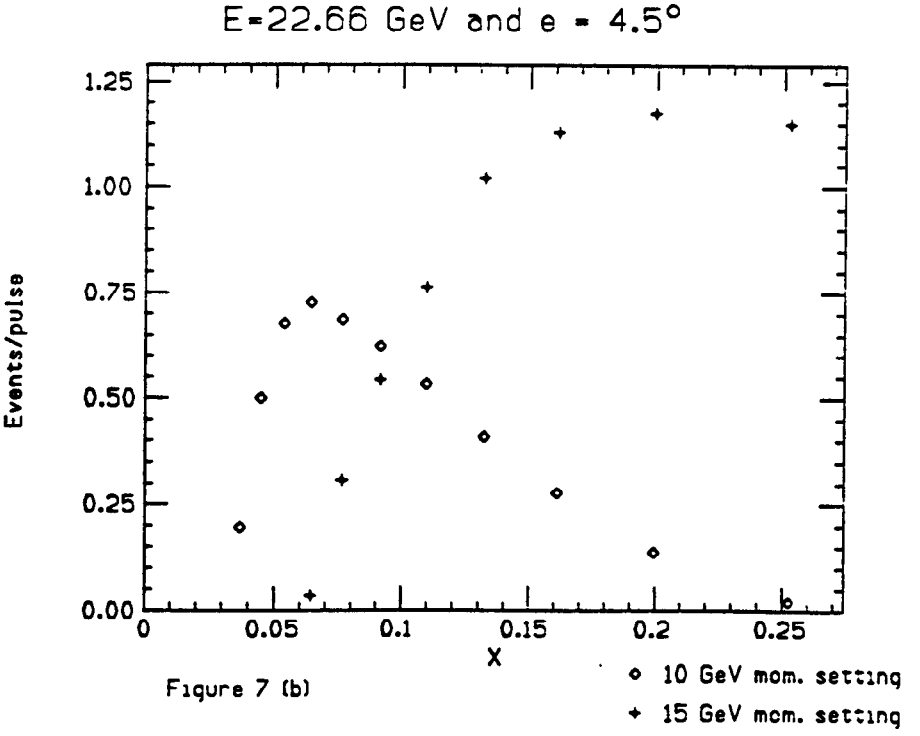

Figure 7 (b)

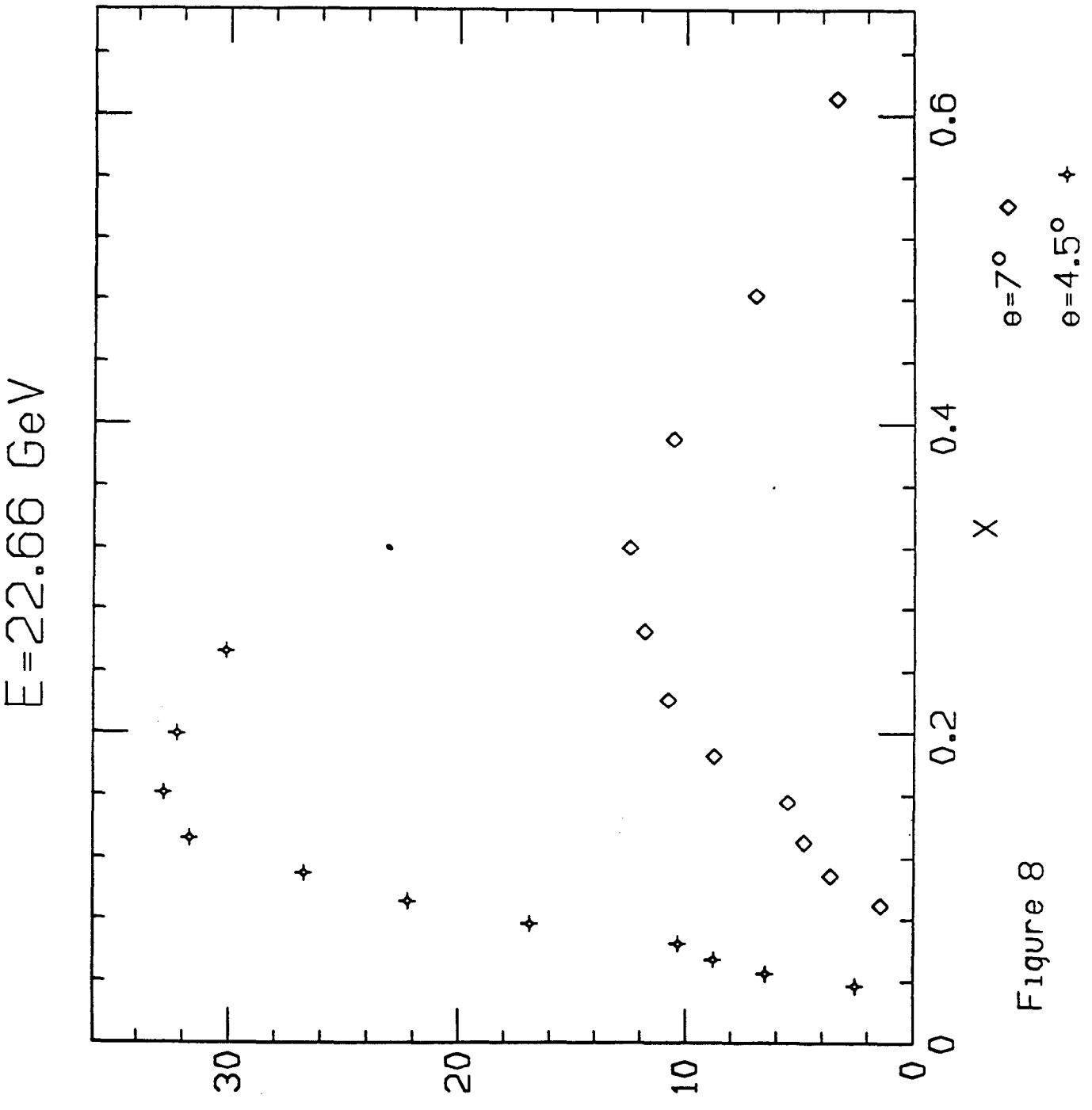

Figure 8

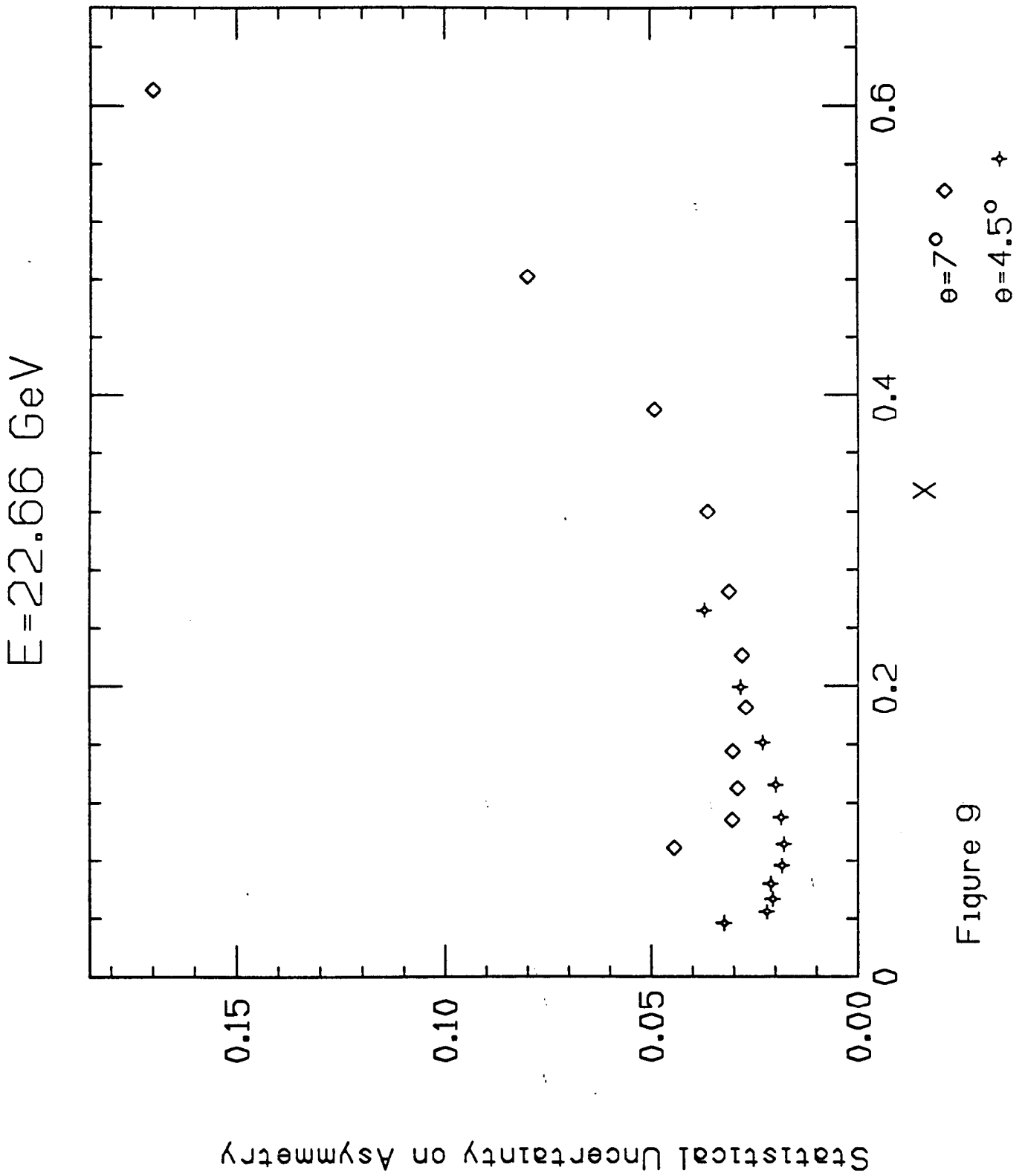
E=22.66 GeV
Statistical Uncertainty on Asymmetry
0.15
0.10
0.05
0.00
0
0.2
0.4
0.6
X
θ=7°
θ=4.5°

Figure 9

SPIN DEPENDENT STRUCTURE FUNCTIONS

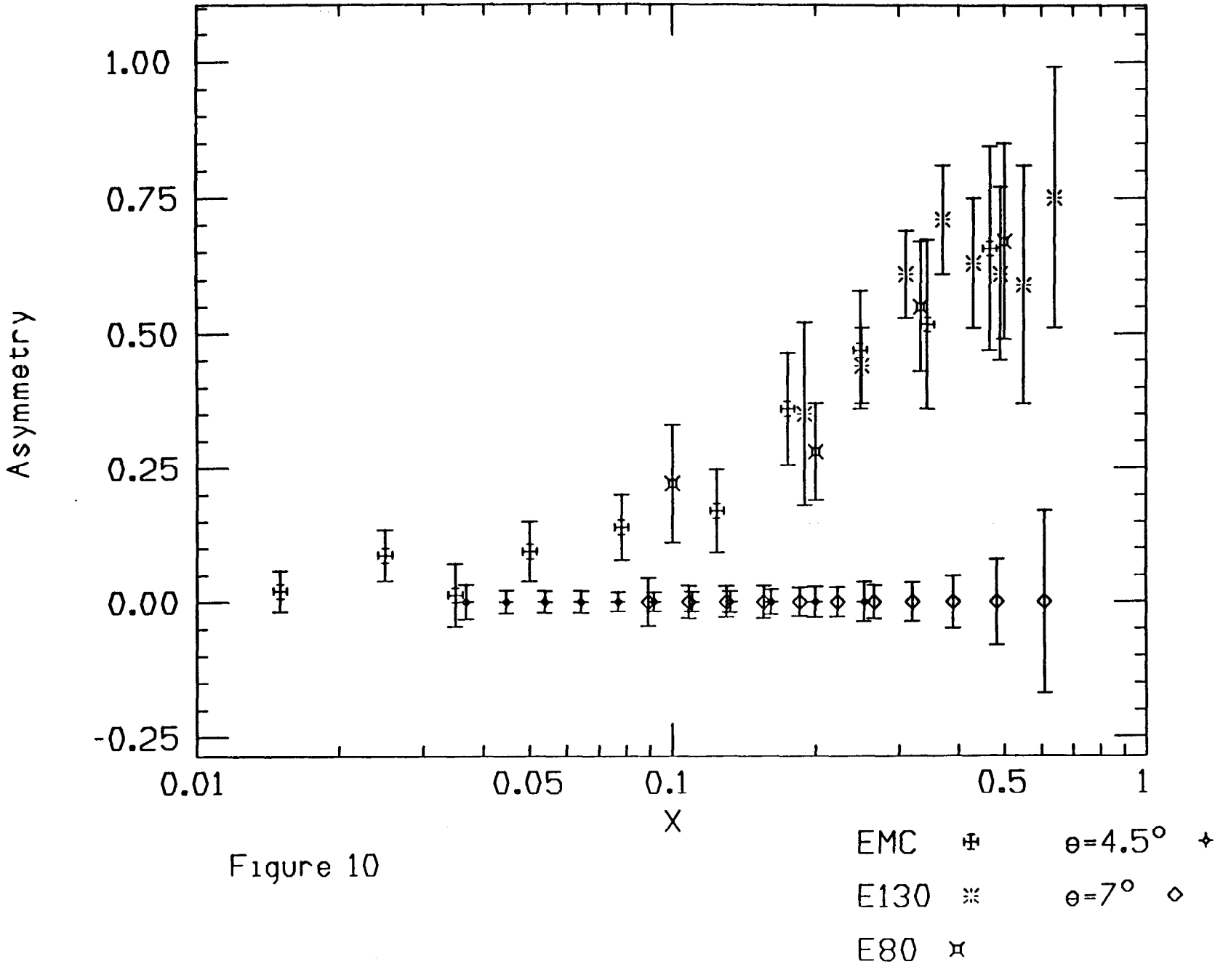

Figure 10

The partial wave channels of the three-nucleon wave function within the Derrick-Blatt scheme

Channel number	L	S	l_a	L_a	P	K	Probability (%)
1	0	0.5	0	0	A	1	87.44
2	0	0.5	0	0	M	2	0.74
3	0	0.5	1	1	M	1	0.74
4	0	0.5	2	2	A	1	1.20
5	0	0.5	2	2	M	2	0.06
6	1	0.5	1	1	M	1	0.01
7	1	0.5	2	2	A	1	0.01
8	1	0.5	2	2	M	2	0.01
9	1	1.5	1	1	M	1	0.01
10	1	1.5	2	2	M	2	0.01
11	2	1.5	0	2	M	2	1.08
12	2	1.5	1	1	M	1	2.63
13	2	1.5	1	3	M	1	1.05
14	2	1.5	2	0	M	2	3.06
15	2	1.5	2	2	M	2	0.18
16	2	1.5	3	1	M	1	0.37

Figure 11

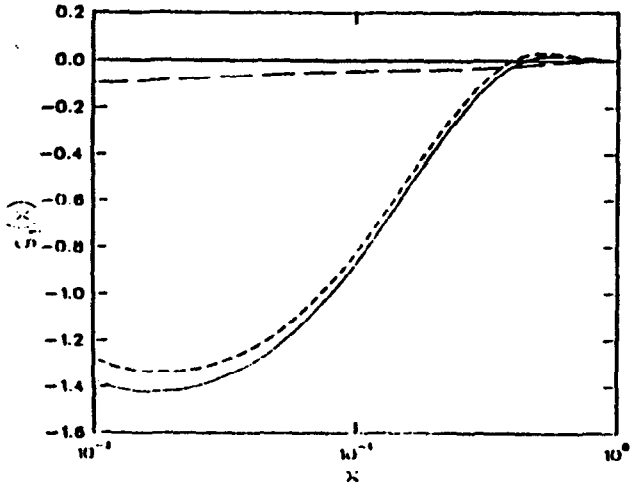

Fig. 13

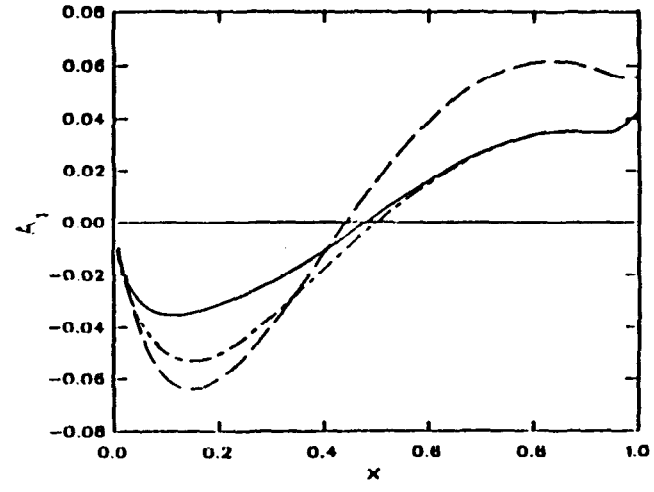

Fig. 15

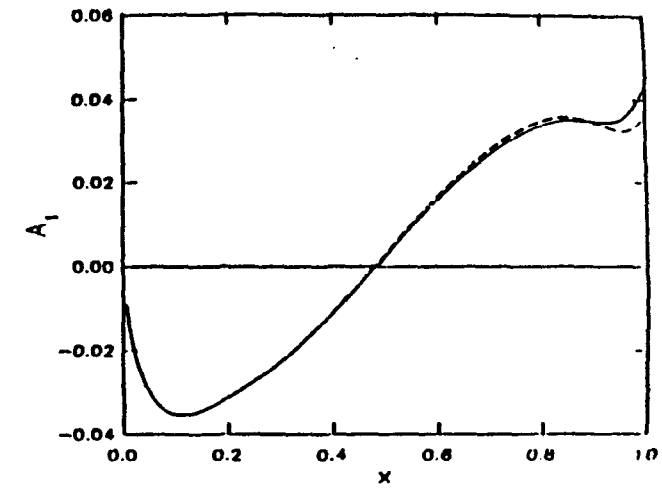

Fig. 17

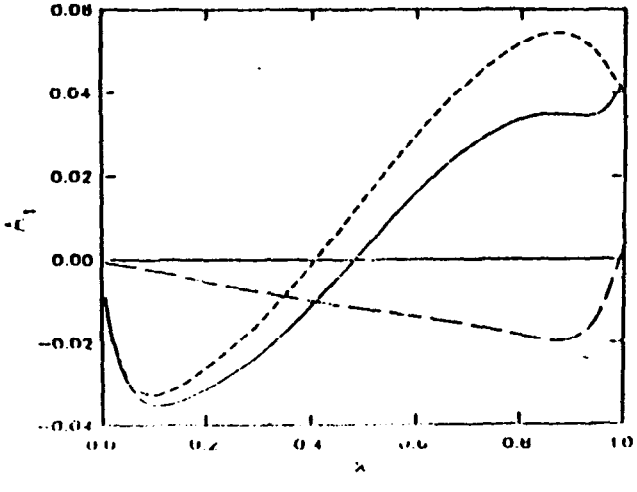

Fig. 14

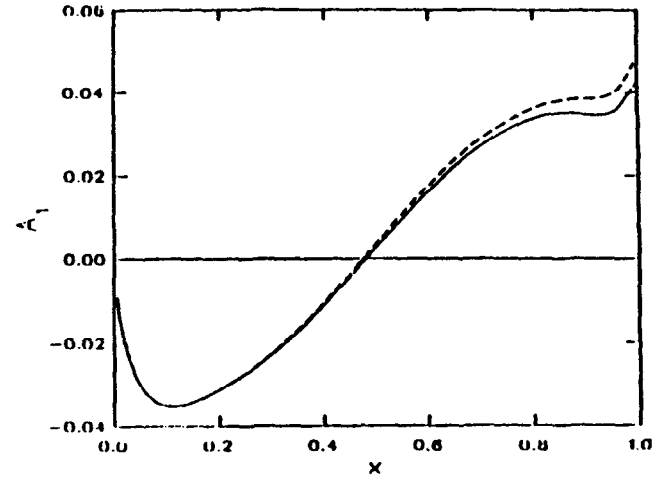

Fig. 16

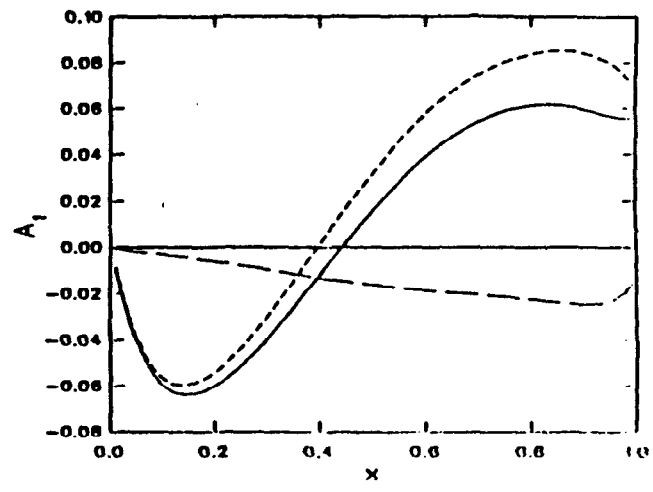

Fig. 12

FIGURE 12 (text)

see next page for figure captions

Figure Captions (preceeding page)

12. Asymmetry A_1 for scattering from polarized ^{3}He calculated in Model I (solid curve) versus x. The short-dashed curve shows the neutron contribution and the long-dashed curve the proton contribution.

13. The structure function g_1 for ^{3}He versus x calculated in Model I (solid curve). Also shown are the separate neutron (short-dashed curve) and proton (long-dashed curve) contributions.

14. Asymmetry A_1 for scattering from polarized ^{3}He at $Q^2 = 10$ (GeV/c)^2 calculated in Model II (solid curve) versus x. The short-dashed curve shows the neutron contribution and the long-dashed curve the proton contribution.

15. Comparison of polarized ^{3}He asymmetry at $Q^2 = 10$ (GeV/c)^2 using Model I (long-dashed curve) and Model II (solid curve). Also shown is the result from Model II if sea quark polarization is omitted (dash-dot curve).

16. Asymmetry A_1 for scattering from polarized ^{3}He versus x showing the effect of different choices of energy in (3.3). The solid curve is calculated using (3.4) and the dashed curve using (3.5).

17. Asymmetry A_1 for scattering from polarized ^{3}He versus x showing the effect of the relativistic normalization factor[25,11]) in eq. (3.2). The solid curve is calculated using eq. (3.2) and the dashed curve is calculated omitting the relativistic normalization factor.